Hot carrier base photovoltaic response of GaSb/InAs Type-II strained-layer superlattice structure in the Terahertz (THz) region

P.K.D.D.P. Pitigala,

Department of Physics, University of Sri Jayewardenepura, Gangodavila, Sri Lanka.

Department of Physics & Astronomy, Georgia State University Atlanta GA

Center for Advance Material Research, University of Sri Jayewardenepura, Gangodavila, Sri Lanka

Corresponding Author *email*: dpitigala@sjp.ac.lk

1. ABSTRACT

Superlattice structures grown with InAs, GaSb and AlSb are known as strained-layer-superlattice structures (SLS). InAs/GaSb SLS have a broken-gap band alignment and a hybridization of conduction-band (CB) states of InAs and valence-band (VB) states of GaSb respectively forming two mini-bands. The device consists of two p-doped InAs/GaSb superlattice absorber layers, thick 2.1 μm and a 2 μm thick, sandwiching a 100nm thick InAs/AlSb superlattice barrier. The terahertz (THz) response with a peak at 2.3 THz (132 μm) operating at temperatures up to ~140 K under photovoltaic operation (i.e., with 0 V applied bias). The highest THz response in the device is observed at 110 K, and has a responsivity of ~50 mA/W with a detectivity (D*) of 7×10^8 Jones. This THz response decreases with increasing applied bias voltage or cutting off MIR irradiation as they deplete the mini barrier or the hot-carriers, respectively; the source of the THz response.

2. INTRODUCTION

Scientists and device engineers are searching for novel material combinations for infrared and terahertz (THz) detectors. InAs, GaSb and AlSb, have gained the attention of device engineers [1] and the superlattice structures grown with InAs, GaSb and AlSb are strained Super Lattice Structures (SLS) due to the small lattice mismatch in materials. InAs/GaSb SLS have broken-gap band alignment and the hybridization of conduction band (CB) states of InAs and valence band (VB) states of GaSb respectively form two mini-bands in SLS [2]. The highest hole mini-band level (HH1) will be generated in the CB-VB overlap region in the InAs/GaSb SLS, and the lowest electron conduction mini-band (C1) will be generated in between the CB overlap region of InAs and GaSb. These HH1 and C1 levels enable carrier (electron and hole) transitions in

SLS. Additionally, they enable band gap tuning via adjusting GaSb and InAs layer thicknesses and number of layers [2]. An InAs/GaSb SLS structure has been reported [3] for far-infrared (FIR) response up to 32 μm with maximum operating temperature ranging from 50 to 65 K. A novel device structure based on 6.1 Å group materials known as nBn structure was reported to reduce the Shockly-Read-Hall effects [4], and hence increase the operating temperature to ~ 150 K [5]. IR detectors made with nBn and pBp based structures have mid-infrared (MIR) responses with threshold wavelengths extending up to 13μm [6].

In this paper we report a THz response observed in a device based on pBp SLS consisting of GaSb/InAs SLS with 0 V applied bias. Usually the THz spectrum is treated as wavelengths from 30 μm to 300 μm (10 to 1 THz), which is overlapping with the FIR region and submillimeter region, i.e., from 30 μm to 100 μm and 100 μm to 3mm in wavelength respectively [7]. THz detectors have gained interest in recent years due to their potential applications in a vast variety of areas ranging from military and defense to civilian applications. In the past two decades, different types of THz detectors including quantum dots [8, 9], quantum rings [10], homojunction [11], p-type [12] and n-type [13] heterojunction devices have been tested, and reported in literature. All these different types of THz detectors require cooling with liquid helium (4.2 K) for best performance. In contrast, only thermal and plasma-wave coupled THz detectors are reported to be operating at high temperatures [7]. The device report here is operating at 110 K, and it will reduce the burden of additional operation cost of the device cooling to very low temperatures, compared to other devices based on photon absorption. Furthermore, our device is operating with 0 V applied bias (photovoltaic mode (PV)), have low power consumption. Furthermore, understanding the mechanism behind the THz response in pBp SLS will broaden the potential use of pBp device's and additionally facilitate on designing SLS structures leading to improved performance such as responsivity, detectivity, and selective THz responses for varies applications.

3. METHODOLOGY

The device tested consists of a 100 nm thick 16 ML InAs/ 4 ML AlSb superlattice structure (ML-monolayers) as a barrier, sandwiched between two absorber layers a 2.1 μm thick 14 ML InAs/ 10 ML GaSb superlattice structure, and a 2 μm thick a 10 ML InAs/ 4 ML GaSb superlattice structure respectively. The two absorber regions were p-doped to 1×10^{16} cm^3 and the two contact layers were p-doped to 4×10^{18} cm^3 and have the same superlattice structure as their adjacent absorber layer 14. The schematic of the device structure and the energy band diagram are shown in Fig. 1. The response of the device was measured with a Perking Elmer System 2000 FTIR calibrated with a silicon bolometer. Current-Voltage (I-V) characteristics were measured using a Keithley 2400 source meter with the device mounted in a closed-cycle refrigerator for temperature variation.

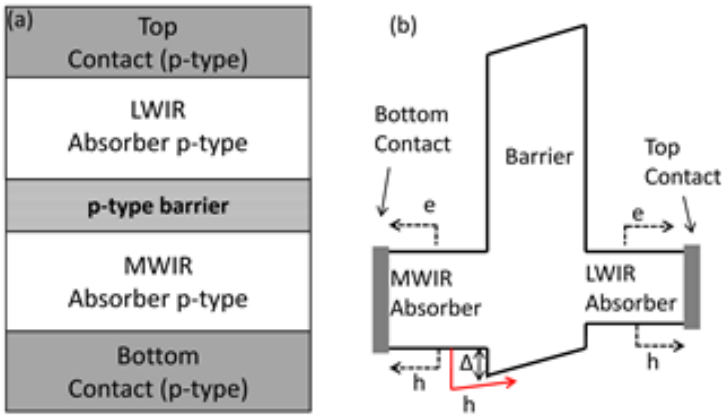

Figure 1. (a) A schematic of the layer structure in the pBp structure. **(b)** The energy band alignment and possible carrier transition paths in the device. Carriers (hot-holes) occupying the HH1 level after initial excited as electron-hole pair in MWIR absorber will overcome the barrier by acquiring energy from THz irradiation result in the THz response (solid line arrow). There is a possibility that both the electrons and holes can contribute in to THz response via excitation over the barrier at the interface of contact regions and the absorber regions (dashed line arrows), but experimental results shows those transitions are not contributing to the THz response.

4. RESULTS AND DISCUSSION

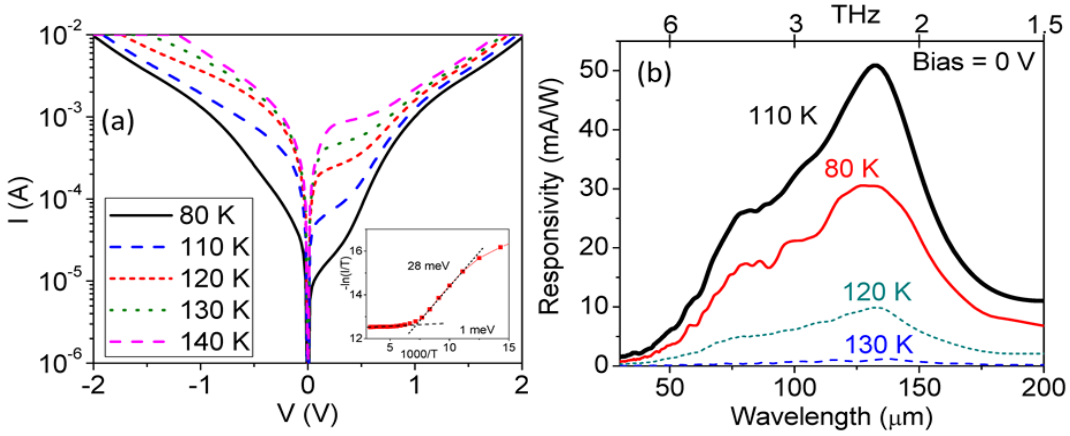

Figure 2. (a) The current-voltage (IV) characteristics of the device under different temperatures. The asymmetry in the IV characteristics is due to the asymmetry due to the LWRI and MWIR absorber layers structure in the device. **(inset)** The Arrhenius plot of the dark current variation vs. the inverse of temperature for the device. A barrier of ~ 28 meV can be observed by the results in 70K to 110K. At higher temperatures the barrier is diminishing. (b) The responsivity spectra of the device at 80K, 110K, 120 K and 130 K with 0V applied bias. The highest responsivity in the THz response is observed at 110 K. The response rapidly decreases with increasing temperature from 110 K to 130K.

I-V characteristics of the device under different temperatures from 80K to 140 K are shown in Fig. 2a. The negative bias in I-V indicates that the positive polarity is applied to the bottom contact (BC) while under positive bias the positive polarity is on the top contact (TC). The asymmetry between the positive and negative bias is due to the energy difference (~50 meV) in the HH1 and C1 energy gaps in the LWIR absorber region compared to MWIR absorber region [13]. As a result, an energy gradient is formed in the corresponding energy bands in the InAs/AlSb SLS barrier region. The gradient in the in the barrier region facilitate carrier transitions across the device without an applied electric field (E-field) [15].

The THz responsivity spectra of the device under different temperatures are shown in Fig. 2b. The response extends from ~30 μm to over 200 μm, and peaks at ~2.3 THz (132 μm). The highest responsivity of ~50 mA/W, at the response peak, was observed when the device is operating at ~ 110 K. The responsivity decreases rapidly as the temperature increases over 110 K and fades away at ~ 140 K with a reduced signal to noise ratio (SNR). The SNR becomes < 1 as the temperature exceeds 140 K. Additionally, activation energy (Δ) of ~ 28 meV is extracted from the Arrhenius plot in the temperature range 60K -120K, and at higher temperatures the Δ reduces to ~ 1 meV as shown in the inset of Fig. 2a. This activation energy corresponds to the HH1 band offset at the MWIR/Barrier interface and the reduction in the activation energy can be the cause for the vanishing THz response with increasing temperature.

The responsivity and the Johnson noise limited detectivity (D*) of the device at different temperatures are tabulated in Table I. The D* is ~7×10^{8} Jones at 110 K, but a higher D* ~ 1.2×109 Jones is observed for 80K due to low Johnson noise at low temperature. Further decreasing the temperature decreases both the responsivity and D* of the device.

Table 1. The responsivity and detectivity (D*) of the pBp structure at THz response peaks (2.3 THz / 132 μm) at different temperatures.

Temperature (K)	Responsivity (mA/W)	Detectivity (D*) (Jones)
80	30.4±0.2	1.2×10^{9}
110	50.8±0.2	7.0×10^{8}
120	9.9±0.4	1.1×10^{8}
130	1.1±0.5	1.1×10^{7}

A diminishing THz responsivity was observed when a bias is applied across the device as shown in Fig. 3a. By applying an bias of ~ 50 mV in the direction from top contact to bottom contact (TC-to-BC) the THz response is reduced by approximately two orders in magnitude, while an bias of ~ 50 mV in the opposite direction (BC-to-TC) reduces the responsivity by approximately three orders in magnitude compared to the 0 V responsivity. Further increase in the bias decreases the Signal to Noise Ratio (SNR) as does with the responsivity at high temperatures. The decreasing SNR with increasing applied bias can be observed in responsivity spectra shown in Fig. 3a.

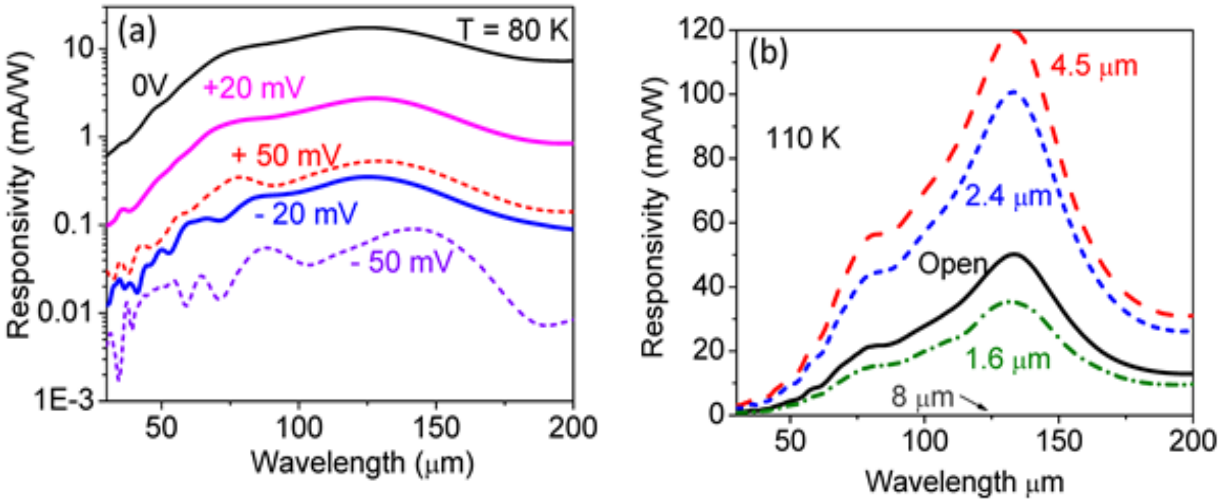

Figure 3. (a) The THz response decreased with a small negative and positive applied bias with respect to the bottom contact. The carrier tunneling due to depletion of the barrier under positive bias and the opposing force applied by the E-field under negative bias can be the cause of decreasing THz response. **(b)** The THz responsivity variation due to MIR irradiation while cutting off short-wavelenth irradiation using different cut-on threshold filters. When an 8 μm cut-on filter is used to cut off the MIR irradiation on to the device the THz response annihilate, while using cut-on filters with 4.5 μm and 2.4 μm thresholds increased the THz response.

Additionally, interesting behaviors in the THz response was observed when NIR and MIR irradiation on to the device were cut-off by long-pass filters as shown in Fig. 3b. The THz response vanished when an 8 μm cut-on filter (50% transmission at 15μm) is used. Most interesting observation was the increase in the THz signal, compared to the signal without any cut-on filters ("open" in Fig. 3b), when using long-pass filters with cut-on thresholds at 4.5 μm and at 2.4 μm. Furthermore, with the 1.6 μm cut-on filter the response decreased below the

“open” response. This observation implies that both the incident radiation intensity as well as the photon energy in the radiation are contributing to the latter described behavior. And more detailed, intensive and thorough study is needed to better understanding the causes of this phenomenon, with considering all the correlations of NIR, MIR and FIR radiation transmission properties of the optics used with the experimental setup.

A carrier transition mechanism to explain the THz response is developed based on the above observations. The requirement of MIR irradiation on generating the THz response in the device indicates that the THz response is assisted by initial carrier (electron-hole pair) excitation on to the HH1 and C1 energy bands in the MWIR or LWIR regions. We have identified three carrier transition processes that may assist PV response. (1) Holes in the MWIR absorber, generated by electron-hole pair production by absorbing MIR photons, directly transfer over the graded barrier. This will produce the MIR response observed in the device (this response is not within the scope of this paper). (2) Holes excited by the process 1, but do not have sufficient energy to directly overcome the barrier can be trapped in the HH1 energy band of the MWIR absorber (hot-holes). These hot-holes can be re-excited by THz photons over the graded barrier, contributing to the photocurrent in the device. (3) The hot-holes or hot-electrons trapped in the HH1 and C1 energy bands of the MWIR (LWIR) absorber region can be re-excited by THz photons over the Schottky barrier at the interface of bottom (top) contact layer as shown by dotted arrows in Fig. 1. The carrier transition through the process 3 can be very small or negligible as there is no energy-gradient formed in the top and bottom contact regions to enable carriers to free flow. Hence the dominant carrier transition process responsible for the THz response should be the process 2.

Furthermore, by cutting off the MIR irradiation only up to 8 μm was able to suppress the THz response. If the carrier excitation in the LWIR absorber is dominating or giving a significant contribution to the THz response, we should be able to observe the THz response even with the 8 μm cut-on filter blocking the partial irradiation spectrum. This observation further confirms the electron-hole pair in the LWIR absorber, hence the process 3, is not contributing or provides only a minimal contribution to the THz response in the device, compared to process 2.

Additionally, the photoresponse spectrum at 0 V bias shown by Plis et. al.[14] has seen a similar profile to their photoresponse from the MWIR absorber under applied bias, but have a slight blue shift (from ~ 10 μm to ~ 8.2 μm) which correspond to ~ 25 meV energy difference in the response threshold due to the additional energy required to overcome the height of the graded barrier for the PV response. This further confirms the existence of process-1 in the device and the PV response in the device is originated by the carrier transitions from the MWIR absorber over the graded barrier.

Furthermore, the THz response annihilation under applied bias is due to BC-to-TC E-field been assisting the carrier tunneling or depleting the graded barrier in the HH1 band. Hence the density of trapped holes in the MWIR HH1 band will deplete. The low rate of decrease in the THz response under increasing positive bias compared to the negative bias is due to the E-filed strength required to enable tunneling, or depletion in the barrier. When the E-field is in the opposite direction, i.e., from TC-to-BC, it opposes the hole transitions from MWIR absorber region on to LWIR, or reduce the gradient of the barrier, so the carrier free flow from MWIR region to LWIR region will be opposed. Both the bias conditions affect the carrier transition process responsible for THz response. Therefore, under applied bias the THz response is weakened or concealed. This observation also supports the argument that carrier transition process 2 is the main cause of THz response in the device.

Analyzing these observations, it can be concluded that THz response in the device is caused mainly by carrier transition due to the gradient in the barrier region via the process-2, and those carriers been collected at the top contact region, or accumulated at LWIR absorber in the pBp SLS generating a potential difference between the TC and the BC region.

5. CONCLUSION

In a summary, we report the THz response observed, under photovoltaic mode (0 V bias) operation, in pBp type structure grown with InAs/GaSb strained-layer superlattice. A THz response have not been observed or reported before in pBp SLS based devices. Understanding the carrier transition process involved in the THz response is important and is useful in further improvement and identification of potential uses of this novel structure. The THz response maximizes at ~110 K and rapidly decreases with increasing temperature as well as applied bias. The THz response expand from 10 THz (30 μm) and extend over 1.5 THz (200 μm) and the response peak is observed at 2.3 THz (132 μm). The THz response is resulted by excitation of hot-holes over the graded barrier, which have trapped and accumulated on the HH1 mini-band in the MWIR absorber regions after initially excited as an electron-hole pair by the MIR irradiation. At ~110 K a responsivity of ~50 mA/W corresponds to a D* of ~ 7×10^8 Jones, at peak wavelength 132 μm was observed in the device. Further studies are needed on understanding the effects observed due to partial MIR irradiation with MIR cut-on filters.

6. ACKNOWLEDGEMENT

The author wish to acknowledge Prof. AGU Perera, Department of Physics and Astronomy, Georgia State University and Prof. S. Krishna and Dr E.A. Plis of Department of Electrical and Computer Science, University of New Mexico, NM for their support and providing of devices samples for this study

7. REFERENCES

[1]. Kroemer H., Physica E: Low-dimensional Systems and Nanostructures 20, (2004).196-203
[2]. Halvorsen, E. Galperin Y. and. Chao K. A, Physical Review B 61 (2000).16743-16749
[3]. Wei Y., Gin A., Razeghi M. and Brown G. J., Applied Physics Letters 81 (2002). 3675-3677
[4]. Maimon S.and Wicks G. W., Applied Physics Letters 89 (2006). 151109-151103
[5]. Khoshakhlagh A., Rodriguez J. B., Plis E., Bishop G. D., Sharma Y. D., Kim H. S.,. Dawson L. R and Krishna S., Applied Physics Letters 91 (2007). 263504-263503
[6]. Ariyawansa G., Grupen M., Duran J. M., Scheihing J. E.,. Nelson T. R and Eismann M. T., Journal of Applied Physics 111 (2012). 073107-073110
[7]. Rogalski A. and Sizov F., Opto-Electron. Rev. 19 (2011). 346-404
[8]. Huang G., Yang J., Bhattacharya P., Ariyawansa G. and Perera A. G. U., Applied Physics Letters 92 (2008). 011117-011113
[9]. Bhattacharya P., Xiaohua S., Ariyawansa G. and Perera A. G. U., Proceedings of the IEEE 95 (2007). 1828-1837
[10]. Bhowmick S., Huang G., Guo W., Lee C. S., Bhattacharya P., Ariyawansa G. and Perera A. G. U., Applied Physics Letters 96 (2010).231103-231103
[11]. Jayaweera P. V. V., Matsik, S. G. Perera A. G. U., Paltiel Y., Sher A., Raizman A., Luo H. and Liu H. C., Applied` Physics Letters 90 (2007). 111109-111103
[12]. Rinzan M. B. M., Perera A. G. U., Matsik S. G., Liu H. C., Wasilewski Z. R. and Buchanan M., Applied Physics Letters 86 (2005). 071112-071113
[13]. Weerasekara A., Rinzan M., Matsik S., Perera A. G U., Buchanan M., Liu H. C., von Winckel G., Stintz ` A.and Krishna S., Opt. Lett. 32 (2007). 1335-1337
[14]. Plis E. A, Krishna S. S., Gautam N., Myers S. and Krishna S., Photonics Journal, IEEE 3 (2011)., 234-240
[15]. Pitigala, P. K. D. D. P. Matsik S. G.,. Perera A. G. U, Khanna S. P., Li L. H.,. Linfield E. H, Wasilewski Z. R., Buchanan M.and Liu H. C., Journal of Applied Physics 111 (2012)., 084505-084505